Perovskite Phases and Phasoids in $Sm_{1-x}Sr_xCuO_{2.5-x/2+\delta}$ PLD Thin Films

B. Mercey, A. Gupta,* M. Hervieu, and B. Raveau

*Laboratoire CRISMAT, CNRS URA 1318-ISMRA, Université de Caen Boulevard du Maréchal Juin, 14050 Caen Cedex, France; and
IBM Research Division, Thomas J. Watson Research Center, Yorktown Heights, New York 10598-0218

The pulsed laser deposition technique has been used for the thin film synthesis of new perovskite-type phases and phasoids in the $Sm_{1-x}Sr_xCuO_{2.5-x/2+\delta}$ systems. The films are grown on [001] $SrTiO_3$ substrates, and are observed to be preferentially oriented, with the c-axis aligned normal to the substrate, and single-phased over a relatively wide composition range ($0.5 \leq x \leq 1$). HREM studies of the films show the presence of a wide variety of structural arrangements as a function of composition which are related to the basic infinite-layer structure of $SrCuO_2$. In addition to an ordered phase for $x = 0.75$, which has been previously reported, other structures which accommodate excess oxygen to partially compensate for the mixed valence are also observed. These include intercalation of oxygen between the $[CuO_2]_x$ layers, introduction of novel rock salt-type ribbons, and double layers of edge-sharing CuO_4 groups. © 1995 Academic Press, Inc.

INTRODUCTION

The recent studies of high T_c superconductors suggest that the exploration of metastable phases may be the key to achieving higher critical temperatures. For this purpose it is imperative that nonequilibrium techniques for the growth of these materials be investigated. Besides high pressure, which has allowed for the bulk synthesis of a number of high T_c superconducting cuprates, the RHEED monitored pulsed laser deposition (PLD) technique is undoubtedly a very promising method for the stabilization of new phases in the form of thin films. The synthesis of metastable perovskites in the RE–Ba–Cu–O (1), La–Ba–Cu–O (2a), and Sr–Ca–Cu–O (2b) systems by PLD supports this viewpoint. The study of cuprates derived from the $Sr_{1-x}Ca_xCuO_2$ structure (3), i.e., involving infinite "CuO_2" layers is of prime importance considering the possibility of achieving critical temperature up to 110 K in defect structures of these compounds (4, 5). With this perspective an investigation of the related system "$SrCuO_2$–$SmCuO_{2.5}$" was recently undertaken (6). For this mixed valence system, it has been possible to stabilize thin films on [001] $SrTiO_3$ substrates with a structure closely related to that of the infinite layer-type cuprate $SrCuO_2$ for x ranging from 0.50 to 1 (6). Nevertheless,

the detailed ED and HREM investigation of one of these compositions, $x = 0.75$, has shown the existence of an orthorhombic supercell "$2ap\sqrt{2} \times 2a_p\sqrt{4} \times 3.66$ Å," that corresponds to a new ordered perovskite $Sm_2Sr_6Cu_8O_{17}$ (7). The latter consists of an intergrowth of $[CuO_2]_x$ and $[Cu_4O_9]_x$ chains running along $[010]_p$.

Preliminary investigations (6) have shown that the detailed nature of the ED patterns varies significantly according to the "x" composition value. Sharp reflections are only obtained for $x = 1$, 3/4, and 2/3, whereas for other x values, streaks and diffuse spots, signatures of order–disorder phenomena, are observed. Moreover, even for $x = 3/4$, coherent domains "$a_p\sqrt{2} \times 2a_p\sqrt{2}$" and "$a_p \times 4a_p$," different from the matrix are evidenced. Thus this system appears as susceptible to generate a wide variety of new phases, whose structural details have to be understood. We report herein on the microstructural characterization of new perovskite phases and phasoids in the $Sm_{1-x}Sr_xCuO_{2.5-x/2+\delta}$ thin films.

EXPERIMENTAL

The conditions of thin films deposition, by RHEED monitored (PLD), were previously described (6) and are summarized in Table 1. X-ray diffraction study was performed with a SIEMENS diffractometer in the normal BRAGG reflection geometry. The electron diffraction study was carried out with a PHILIPS EM420 electron microscope operating at 120 kV and high resolution electron microscopy (HREM) was performed with a TOPCON 002B electron microscope having a resolution point of 1.8 Å.

RESULTS AND DISCUSSION

The ED investigation of the system $Sm_{1-x}Sr_xCuO_{2.5-x/2+\delta}$ (6) is summarized in Fig. 1. One observes that besides the orthorhombic perovskite $Sm_2Sr_6Cu_8O_{17}$ ($x = 3/4$) (7), with "$2a_p\sqrt{2} \times 2a_p\sqrt{2} \times 3.66$ Å," there exist for $x = 1$ and $x = 2/3$ two other perovskites characterized by well-resolved spots. Both of them exhibit a tetragonal
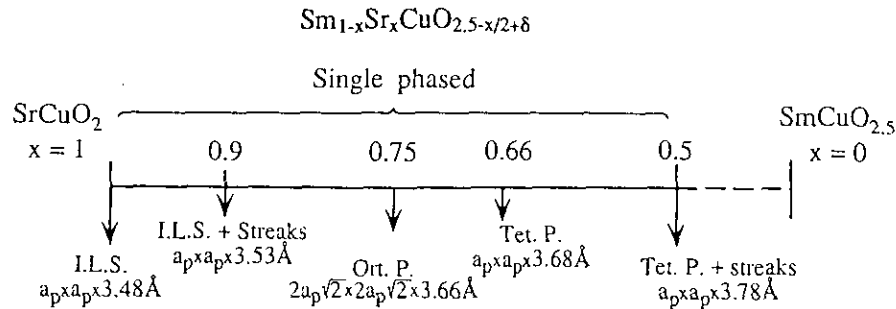
$$Sm_{1-x}Sr_xCuO_{2.5-x/2+\delta}$$

Single phased

SrCuO₂ ⎧⎯⎯⎯⎯⎯⎯⎯⎯⎯⎯⎯⎯⎯⎯⎯⎯⎯⎯⎯⎯⎯⎯⎯⎯⎯⎯⎯⎯⎯⎯⎯⎯⎯⎯⎯⎯⎯⎫ SmCuO₂.₅
x = 1   0.9   0.75   0.66   0.5   x = 0

I.L.S. + Streaks   Tet. P.
I.L.S. $a_p×a_p×3.53$Å   Ort. P. $a_p×a_p×3.68$Å   Tet. P. + streaks
$a_p×a_p×3.48$Å $2a_p\sqrt{2}×2a_p\sqrt{2}×3.66$Å $a_p×a_p×3.78$Å

FIG. 1. $Sm_{1-x}Sr_xCuO_{2.5-x/2+\delta}$ homogeneity range: ED and XRD results vs x in the single-phased domain ($1 \leq x \leq 0.5$); ILS indicates the infinite layer structure, Ort. P indicates the orthorhombic perovskite, and Tet. P indicates the tetragonal perovskite.

unit cell, with lattice parameters "$a_p × a_p × 3.48$ Å" and "$a_p × a_p × 3.68$ Å," respectively. For all the other compositions of the single phase region corresponding to $0.50 \leq x \leq 1$, one observes diffuse streaks, in the ED patterns, indicating the presence of some sort of disorder in the structure. It is also observed that the c parameter of the cell, which is aligned normal to the plane of the substrate increases continuously from 3.48 to 3.78 Å as x decreases from 1 to 0.50.

The Infinite Layer Structure SrCuO₂(x = 1)

For $x = 1$, i.e., SrCuO₂, the reconstruction of the reciprocal space from the sharp reflections of the ED patterns (Fig. 2a) allows the tetragonal cell parameters to be determined, i.e., $a \approx 3.9$ Å, $c = 3.45$ Å, which is in agreement with the XRD patterns (Fig. 3a). These results show that c is perpendicular to the substrate (Fig. 4). The HREM images exhibit an even contrast (Fig. 2b), characteristic of the infinite layer structure. Moreover, it is apparent that the $[CuO_2]_\infty$ layers are parallel to the substrate plane and do not exhibit any defects. This is in contrast to previous results (8) for which Sr_2CuO_3-type defects were observed.
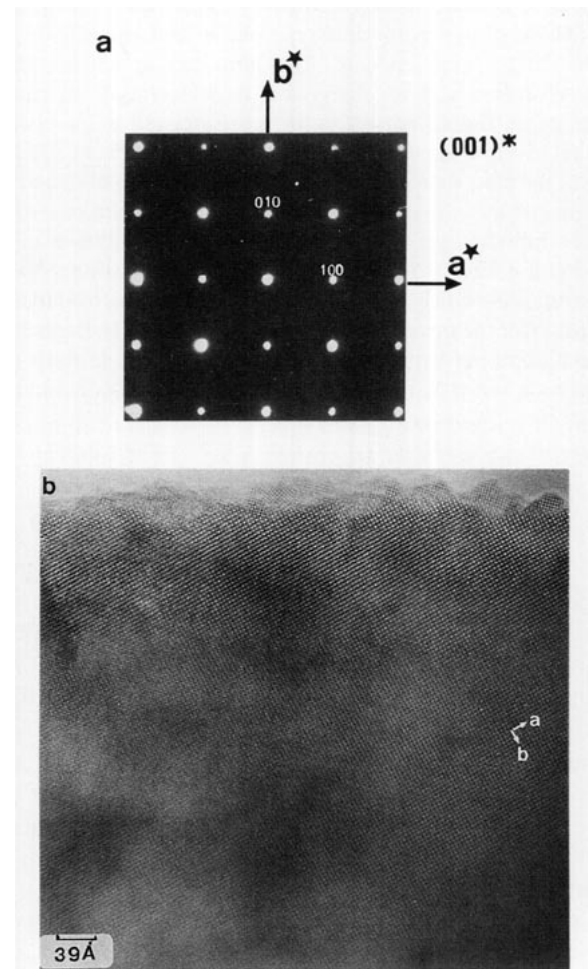
TABLE 1

$Sm_{1-x}Sr_xCuO_{2.5-0.5x+\delta}$ Thin Film Deposition Conditions (1)

Technique	RHEED monitored PLD
Laser	KrF: $\lambda = 248$ nm, 4 Hz, 2 to 3 J cm⁻² at the target
Targets	Orthorhombic SrCuO₂ Mixture of Sm_2CuO_4 and CuO (Sm/Cu = 1)
Oxygenation source	Continuous flow of atomic oxygen and pulsed molecular oxygen source
Mean pressure	1 to 2 10⁻³ Torr
Substrate	[001] SrTiO₃ coated with SrCuO₂
Substrate temperature	600°C
Film thickness	500–700 Å

FIG. 2. SrCuO₂ ($x = 1$) infinite layer structure; (a) [001] ED pattern; (b) [001] HREM image (the films are defect free).

The Tetragonal Perovskite $SmSr_2Cu_3O_{6.5+\delta}(x = 2/3)$

As pointed out above, the reflections of the [001] ED pattern of this phase are sharp (Fig. 5) and no diffuse streaks are observed. The reconstruction of the reciprocal space, allows a tetragonal cell to be evidenced ($a = b \approx$
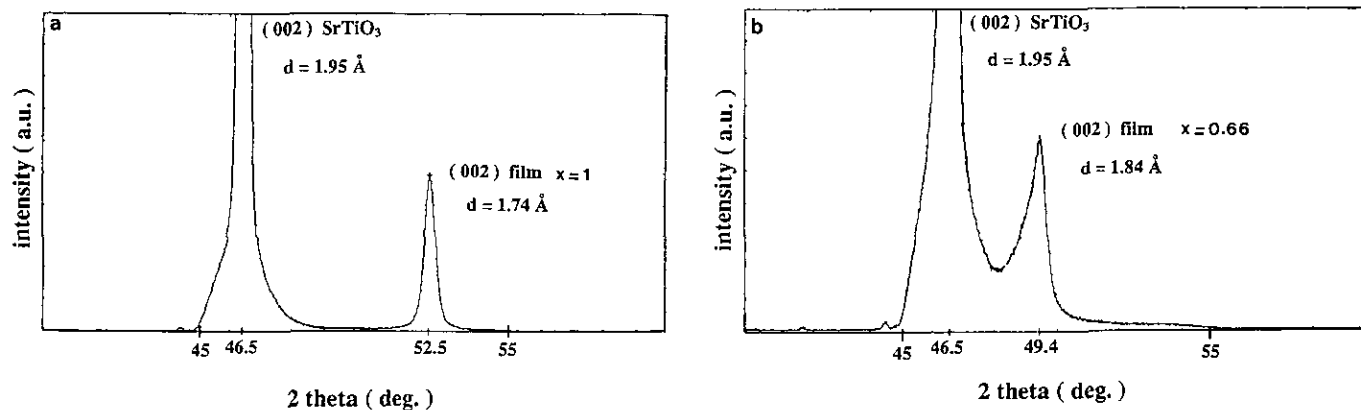
FIG. 3. Expanded XRD patterns with $40° < 2\theta < 60°$ recorded for (a) $SrCuO_2$, ILS, on [001] $SrTiO_3$, and (b) $SmSr_2Cu_3O_{6.5+\delta}$, Tet. P, on [001] $SrTiO_3$.

3.9 Å and $c = 3.68$ Å), in agreement with the XRD pattern (Fig. 3b), and confirms that the c parameter is perpendicular to the substrate.

The HREM images (Fig. 6) display a regular array of white spots spaced of 2.75 Å, without the presence of any local superperiodicity (Fig. 6b). This is in agreement with the contrast expected from the sharpness of the reflections. Note that the effect of film strain (Fig. 6a), attributed to the mismatch between the substrate and the film is not very pronounced. Thus, the overall contrast of the matrix suggests that, in this tetragonal phase, the $[CuO_2]_\infty$ layers are stacked along c in a similar manner as in the infinite layer structure, $SrCuO_2$, with an average spacing of 3.68 Å. However, between the layers additional oxygen atoms are quite likely randomly distributed over the available anionic sites, with the Sm^{3+} and Sr^{2+} also being statistically distributed over the cationic site (Fig. 7a). With the presence of additional oxygen between the layers, the $[CuO_2]_\infty$ layers may also be themselves oxygen deficient, leading to a different orientation of the CuO_5 pyramids (Fig. 7b), as has been observed for example for $x = 0.75$ (7).

Besides the even contrast, characteristic of the whole matrix, local contrast variations are observed in some areas of the micr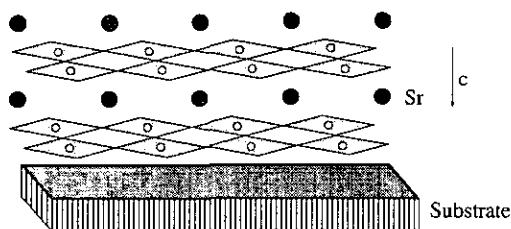ograph. The latters appear in the form of single short rows or groups of select rows of several angstroms that fit in with the matrix (arrowed in Fig. 6c). Such a phenomenon is characteristic of a variation of the atomic distribution in these regions with respect to the surrounding matrix. Taking into account the high oxygen deficiency of this perovskite, i.e., "$O_{6.5+\delta}$" instead of "O_9," this feature is most likely related to a local ordering of the vacancies between the $[CuO_2]_\infty$ layers, which may result in the local association of CuO_5 pyramids. A local ordering of the Sm^{3+} and Sr^{2+} ions may also be associated with this phenomenon leading for instance to the local structure $SmSrCu_2O_5$ (isotypic with $YBaFeCuO_5$ (9) (Fig. 7c).

In any case, it is important to note that $SmSr_2Cu_3O_{6.5+\delta}$ exhibits a different arrangement as compared to $YBa_2Cu_3O_{7-\delta}$ in spite of its identical "123" stoichiometry. In addition, one must point out the possible stabilization of a cubic perovskite ($a = 3.86$ Å), by the PLD technique during the fabrication of $YBa_2Cu_3O_7$ thin films (1). Such a cubic perovskite was never observed in the case of $SmSr_2Cu_3O_{6.5+\delta}$.

FIG. 4. Idealized drawing of the $SrCuO_2$, ILS, deposited on [001] $SrTiO_3$; the c-axis is perpendicular to the substrate.
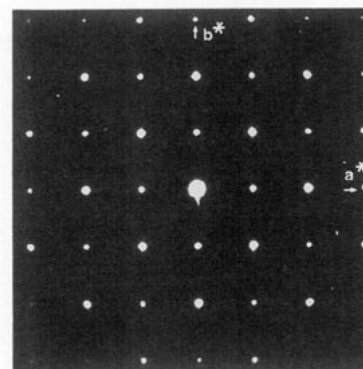
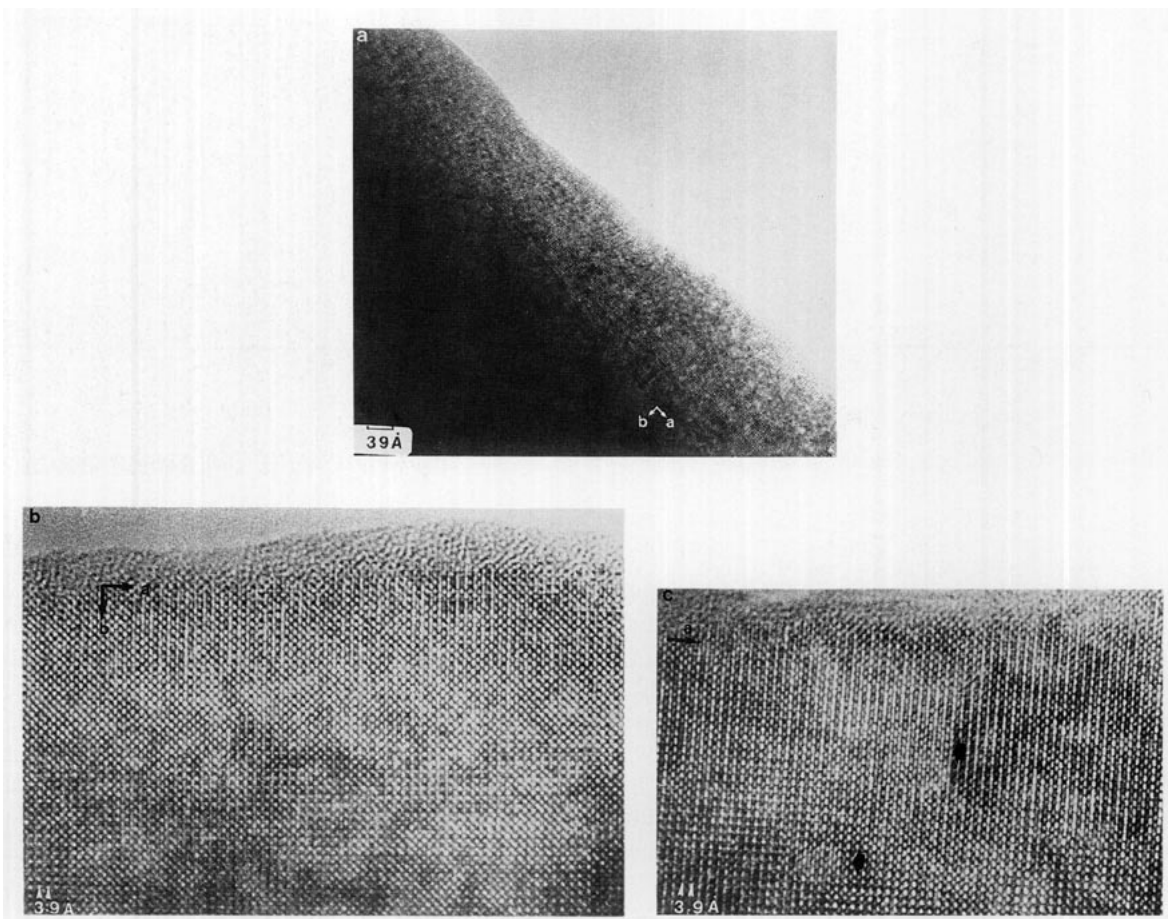

FIG. 5. $SmSr_2Cu_3O_{6.5+\delta}$, tetragonal perovskite [001] ED pattern.

FIG. 6. [001] HREM images of $SmSr_2Cu_3O_{6.5+\delta}$ thin film: (a) overall image showing the absence of defect; (b) enlargement of the image showing a regular array of 2.75 Å spaced white spots; and (c) an example of small areas where the contrast is locally modified (the rectangular domains are indicated by arrows).

Extended defects are observed in some regions of the matrix. These most likely result from nonstoichiometry mechanisms, as they are also evidenced for $0.50 \leq x < 2/3$.

Introduction of Double Zigzag $[(Sm,Sr)O]_\infty$ Layers: The Phasoids $(SrCuO_{2+y})_m(Sm_2CuO_4)_n$ ($0.5 \leq x < 2/3$).

The films remain single phased for $0.50 \leq x < 2/3$. The XRD study shows that the structure is always a tetragonal perovskite, with the c parameter aligned perpendicular to the plane of the substrate, increasing to 3.82 Å for $x = 0.50$. However, all the [001] ED patterns exhibit diffuse streaks, lying along [100]* and [010]*, as shown in Fig. 8. The corresponding images show that the matrix is characteristic of the perovskite phase but is striated by numerous defects running along **a** or **b**, distributed throughout the whole film (Fig. 9a). The magnified images (Fig. 9b) show that such defects consist of double rows of white spots, forming infinite zigzag chains, built up of 90° oriented branches that run along the $\mathbf{a}_p$ and $\mathbf{b}_p$ direc-

tions of the perovskite cell. These defects can be correlated to the formation of double "Sm/Sr" layers that zigzag in the perovskite matrix.

Such double layers of Sm/Sr cations that alternate with copper layers may correspond either to double fluorite-type layers $[Sm_2O_2]_\infty$ as in Sm_2CuO_4 (10) or to rock-salt-type layers $[(Sr, Sm)_2O_2]_\infty$ as in Sr_2CuO_3 (11) or in La_2CuO_4 (12). Thus, two models can be proposed (Fig. 10) to explain the zigzag junction between $SrCuO_2$-type blocks. The first, involving 90° oriented SrO-type layers (Fig. 10a), does not affect the copper coordination. In this model, the rock salt layers exhibit some similarity with $[(Sr, Nd)O]_\infty$ layers encountered in $SrNdCuO_{3.5}$ (13) and $Sr_6Nd_3Cu_6O_{17}$ (14), so that the junction would contain Sm^{3+} and Sr^{2+} cations simultaneously. The second model that consists of 90° oriented fluorite-type layers (Fig. 10b), implies for copper the coexistence of at least three coordinations: pyramidal, tetrahedral, and square planar. The simulated images, calculated for the atomic positions of Sr_2CuO_3 and Sm_2CuO_4, show that in fact few defocus
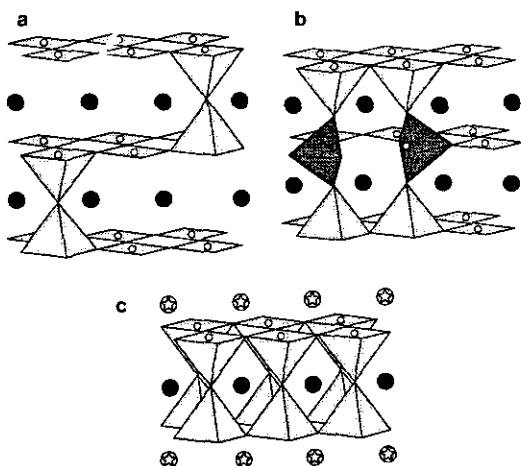
FIG. 7. Idealized drawing of the structure of (a) tetragonal perovskite, "Tet. P," $SmSr_2Cu_3O_{6.5+\delta}$ deduced from the infinite layer structure by the random intercalation of extra oxygen between the $[CuO_2]_x$ layers. Sm^{3+} and Sr^{3+} are statistically distributed over the same cationic site; (b) the presence of oxygen vacancies in the $[CuO_2]$ layers involves the formation of CuO_5 pyramids, the basal plane of which are perpendicular to the substrate; (c) theoretical $SrSmCuO_5$ ordered structure, isotypic with $YBaFeCuO_5$, corresponding to a double ordering of Sr (black dots) and Sm (circled stars) cations in one site and oxygens and vacancies in the other.

FIG. 8. The [001] ED pattern of $Sm_{0.5}Sr_{0.5}CuO_{2.25+\delta}$ ($x = 0.5$) exhibits the reflections of the tetragonal perovskite and streaks lying along $\mathbf{a}^*$ and $\mathbf{b}^*$.

values allow the differentiation of the two models as can be done in a regular structure. Unfortunately, the comparison of the theoretical and experimental images appears unrealistic owing to the local contrast variations which are observed in this disturbed perovskite matrix. Nevertheless, the second model, of the fluorite type layers, appears less probable considering the fact that it would lead to a higher distortion of the copper framework, especially for the CuO_4 tetrahedra (Fig. 10b). On the other
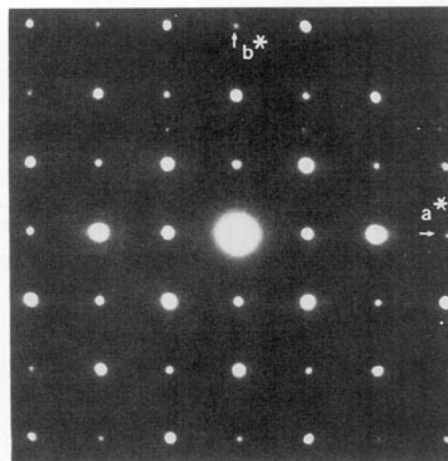
hand, mixed $[(Sr, Nd)O_{1-\varepsilon}]$ rock salt layers have been found to accommodate the oxygen deficiency more readily (13).

It is interesting to note that, as a local arrangement, we often observed groups of parallel $[(Sm, Sr)_2O_2]$ double layers which are spaced by 10 or 13.8 Å, i.e., separated by two or three copper layers, respectively (white arrows in Fig. 9a). These defects can be described by the intergrowth of rock salt and oxygen deficient perovskite layers, according to the general formulation: $[(Sr, Sm)Cu O_{2+y}]_m[(Sr, Sm)_2CuO_4]_n$. The tetragonal perovskite is the limit member $n = 0$ of the family and the local members with $c = 10$ and 13.8 Å (Fig. 9a) are the $m = 1, n = 1$ (or 0212) and $m = 2, n = 2$ (or 0223) members, respectively.

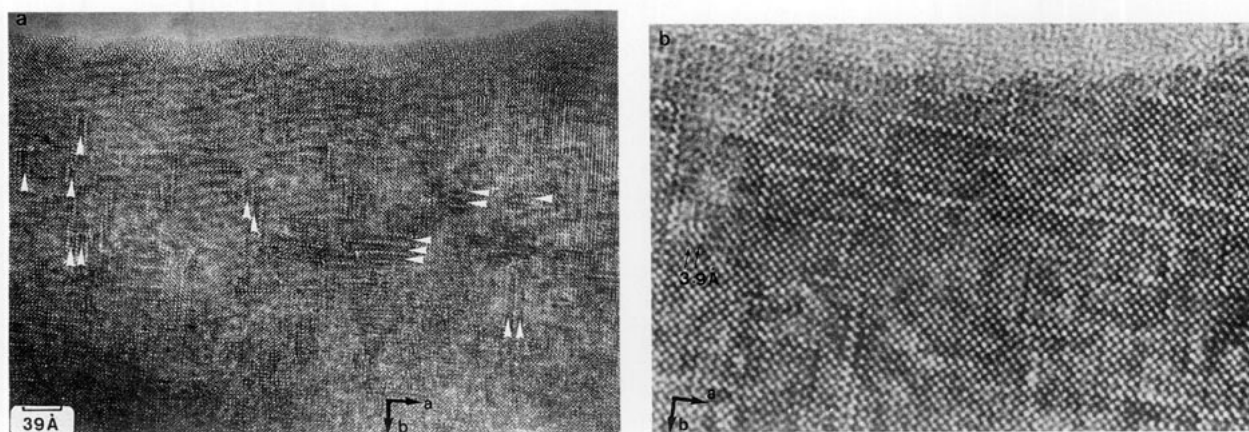In several isolated regions of the crystals, one observes

FIG. 9. [001] HREM images of $Sm_{0.5}Sr_{0.5}CuO_{2.25+\delta}$: (a) overall images showing the presence of numerous defects striating the matrix parallely to $\mathbf{a}$ or $\mathbf{b}$. Note that numerous defect layers are spaced 10 Å apart; some examples are marked by white arrowheads; (b) enlarged image showing the nature of the defects which consist of double $[(Sr, Sm)_2O_2]_x$ layers, zigzagging in the matrix.
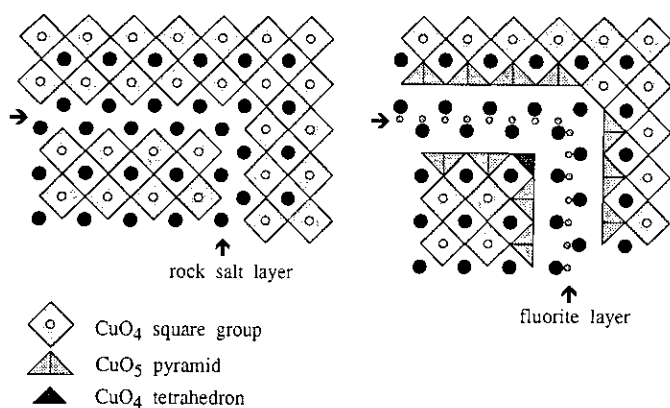
FIG. 10. Idealized models proposed for the double Sm/Sr layers: (a) Rock salt-type which does not modify the copper coordination; (b) Sm_2CuO_4-type which involves, at least, the coexistence of three copper coordinations.

the formation of domains (Fig. 11). The SAED pattern (Fig. 11a) consists of the superposition of two sets of reflections. The first one, denoted as p, corresponds to an "$a_p \times a_p$" cell without reflection condition, whereas the second one, denoted as s, exhibits an "$a_p \times 12$ Å" l-type cell with $k + l = 2n$. The second phase can then be considered as corresponding to the Nd_2CuO_4-type structure. It is quite likely that in this structure samarium is partly replaced by strontium, leading to $Sm_{2-x}Sr_xCuO_{4-x/2+\delta}$, which corresponds to the $m = 0$ member of the family $[(Sr, Sm)CuO_{2+y}]m[(Sr, Sm)_2CuO_4]_n$. This viewpoint is supported by the existence of the isotypic $Nd_{1.9}Sr_{0.1}CuO_4$ (16). The corresponding HREM image (Fig. 11b) shows clearly the transition from the "$a_p \times a_p$" matrix characterized by numerous defects (labeled P

in the right part of the image) to the "$a_p \times 12$ Å" Sm_2CuO_4-type domain (labeled S in the left part of the figure).

90° Oriented Rock Salt and Orthorhombic $SrCuO_2$-type Defects ($x = 0.90$)

For $x = 0.9$, the XRD pattern is similar to that recorded for $x = 1$, with a slightly longer c parameter. However, weak and diffuse streaks are observed along a^* and b^* directions in the ED pattern (Fig. 12a). The HREM image (Fig. 12b) shows the presence of small defect regions scattered over the whole area.

Here again, one observes the formation, in the tetragonal $SrCuO_2$ matrix, of double rock-salt-type defects that appear in the form of rows of dark spots. These are some tens of angströms long (see the black arrowheads parallel to b), with the rock salt ribbons stacked with the copper ribbons (rows of white spots) with a spacing of about 50 Å. In contrast to the boundaries of double cations observed in the $x = 0.50$–0.60 samples, these ribbons do not form 90° oriented infinite zigzag layers. The rock salt layer is abruptly interrupted after a distance of about 20 Å along b, and a new defect appears oriented at 90° which forms rows of white dots (see the white arrowheads parallel to a). This results in the formation of rectangles whose rows of bright dots are shifted $b_p/2$ with respect to the rest of the matrix. Such defects can easily be interpreted as a combination of rock salt-type ribbons with double copper ribbons of edge-sharing CuO_4 square planar groups, as shown in Fig. 13. It is worth pointing out that such double rows of edge-sharing CuO_4 square planar groups are characteristic of the structure of the classical form of the orthorhombic $SrCuO_2$ phase that can be prepared as a bulk material under normal conditions.

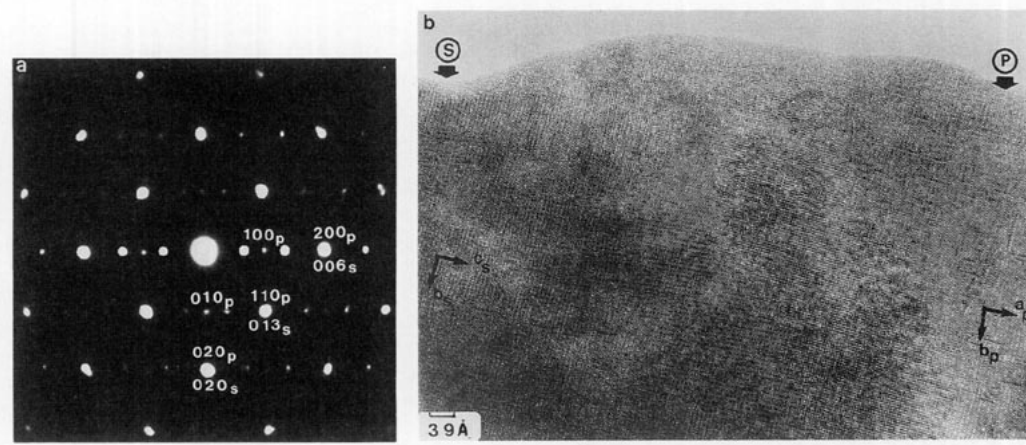It is also remarkable that the introduction of rock salt

FIG. 11. Example of the existence of a small Sm_2CuO_4-type domain (labeled S) in the tetragonal perovskite matrix (labeled P): (a) SAED pattern showing the superposition to the two sets of reflections; (b) [001] image; the Sm_2CuO_4-type domain (s) is observed on the left of the image whereas the tetragonal perovskite matrix (p) is observed in the right, striated by defects characteristic of $0.5 \leq x < 0.66$.
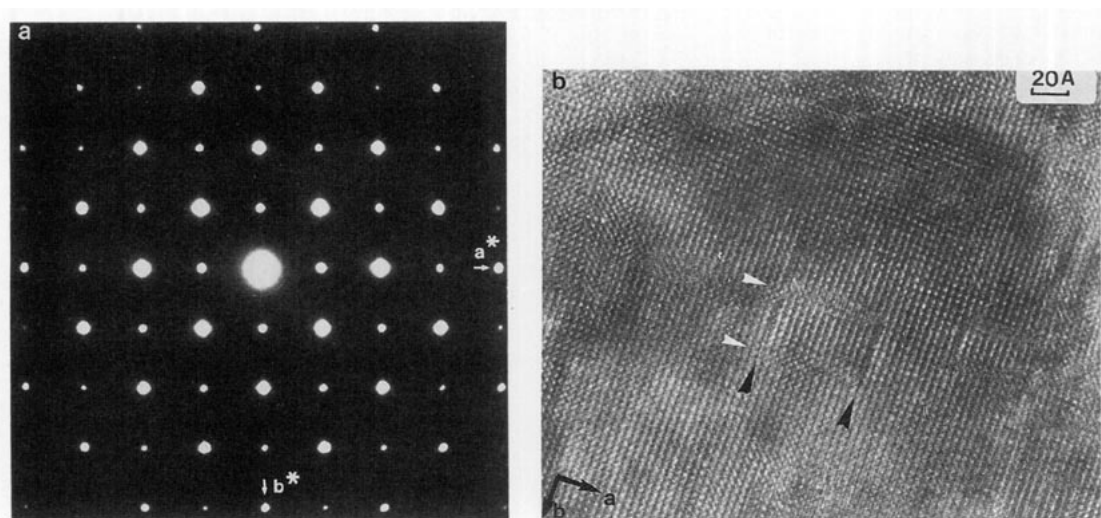
FIG. 12. $Sm_{0.1}Sr_{0.9}CuO_{2.05+\delta}(x = 0.1)$ thin film: (a) the [001] ED pattern exhibits the reflections of the ILS and streaks along a^* and b^*; (b) enlarged image showing the defects parallel to a and b. One rectangle formed by the two types of defective layers is marked by black and white arrowheads. Black arrowheads indicate the double $[(Sr, Sm)O]_x$ layers, whereas the white ones indicate the double copper layers.

layers with double copper layers of edge-sharing CuO_4 square planar groups simultaneously allows the cationic ratio (Sr + Sm)–Cu to be maintained at 1 in agreement with the formulation $Sm_{0.1}Sr_{0.9}CuO_{2.05+\delta}$.

CONCLUDING REMARKS

This study shows the remarkable ability of the PLD technique to synthesize thin films of new perovskite phases and phasoids $Sm_{1-x}CuO_{2.5-x/2+\delta}$, with a variety of structural arrangements derived from the basic infinite layer structure $SrCuO_2$.

In addition to the intercalation of oxygen between the $[CuO_2]_x$ layers, the possibility to accommodate rock salt-type ribbons and double layers of edge-showing CuO_4

groups, as well as other original ordering phenomena as shown for $Sm_2Sr_6Cu_8O_{17+\delta}$ (7) suggest that it should possible to synthesize many other metastable cuprates, including those which exhibit superconductivity, using the PLD technique.

REFERENCES

1. J. F. Hamet, B. Blanc Guilhon, A. Taffin, B. Mercey, M. Hervieu, and B. Raveau, *Physica C* **214**, 55 (1993).
2. R. Desfeux, J. F. Hamet, B. Mercey, Ch. Simon, M. Hervieu, and B. Raveau, *Physica C* **211**, 205 (1993); (b) A. Gupta, B. W. Hussey, T. M. Shaw, A. M. Guloy, M. Y. Chern, R. F. Saraf, and B. A. Scott, *J. Solid State Chem.*, in press.
3. T. Siegrist, S. Zahurac, D. W. Murphy, and R. S. Roth, *Nature* **334**, 231 (1988).
4. M. Azuma, Z. Hiroi, M. Takano, Y. Bando, and Y. Takeda, *Nature*, **356**, 775 (1992).
5. M. Takano, M. Zuma, Z. Hiroi, Y. Bando, and Y. Takeda, *Physica C* **176**, 441 (1991).
6. A. Gupta, B. Mercey, M. Hervieu, and B. Raveau, *Chem. Mater.* **6**(7), 1011 (1994).
7. B. Mercey, A. Gupta, M. Hervieu and B. Raveau, *J. Solid State Chem.*, in press.
8. N. Sugri, M. Ichikawa, K. Hayashi, K. Kubo, K. Yamamoto, and H. Yamouchi, *Physica C* **213**, 345 (1993).
9. L. Er Rakho, C. Michel, Ph. Lacorre, and B. Raveau, *J. Solid State Chem.* **73**, 53 (1988).
10. I. S. Shaplygin, B. G. Kahhan, and W. B. Lazarev, *Russ. J. Inorg. Chem.* **24**, 820 (1979).
11. C. L. Teske and H. K. Müller Buschbaum, *Z. Anorg. Allg. Chem.* **371**, 325 (1969).
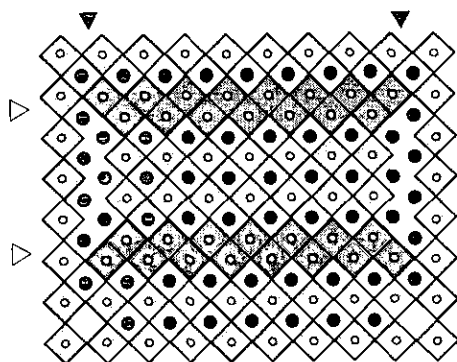

FIG. 13. [001] idealized projection of the defects characterized by two types of double layers. Hatched squares correspond to CuO_4 groups; they are darkened at the level of the double copper layers. Black dots are Sm or Sr ions.

12. H. K. Müller Buschbaum and W. Wollschlager, *Z. Anorg. Allg. Chem.* **414,** 76 (1975).
13. Ph. Labbé, M. Ledésert, V. Caignaert, and B. Raveau, *J. Solid State Chem.* **91,** 362 (1991).
14. V. Caignaert, R. Retoux, C. Michel, M. Hervieu, and B. Raveau, *Physica C* **167,** 483 (1990).
15. V. Caignaert, R. Retoux, C. Michael, M. Hervieu, and B. Raveau, *J. Solid State Chem.* **91**(1), 41 (1991).
16. J. Gopalakrishan, M. A. Subramaniam, C. C. Torardi, J. P. Attfield, and A. W. Sleight, *Mater. Res. Bull.* **24,** 321, (1989).
17. H. Takagi, S. Uchida, and Y. Tokuro, *Phys. Rev. Lett.* **62,** 1197 (1989).